Corrosion Science 101 (2015) 12–18

Contents lists available at ScienceDirect

Corrosion Science

journal homepage: www.elsevier.com/locate/corsci

Hydrogen embrittlement of ultra high strength 300 grade maraging steel

L.P.M. Santos [a], M. Béreš [a], I.N. Bastos [b], S.S.M. Tavares [c], H.F.G. Abreu [a], M.J. Gomes da Silva [a,*]

[a] Universidade Federal do Ceará, Departamento de Engenharia Metalúrgica e de Materiais, Campus do Pici, Av. Humberto Monte, CEP 60445-554 Fortaleza, CE, Brazil
[b] Universidade do Estado do Rio de Janeiro, Instituto Politécnico, Rua Bonfim, 25, CEP 28625-570 Nova Friburgo, RJ, Brazil
[c] Universidade Federal Fluminense, Departamento de Engenharia Mecânica, Campus da Praia Vermelha, Rua Passo da Pátria, CEP 24210-240 Niterói, RJ, Brazil

ARTICLE INFO

Article history:
Received 26 February 2015
Received in revised form 16 June 2015
Accepted 17 June 2015
Available online 27 June 2015

Keywords:
Maraging steels
Hydrogen embrittlement (HE)
Slow strain rate testing (SSRT)

ABSTRACT

Slow strain rate tests were conducted in air and aqueous 0.6 M NaCl at −1.2 V_{SCE} environments to investigate hydrogen embrittlement (HE) of ultra high strength 300 grade maraging steel. The results showed that the samples were susceptible to HE in different levels after submitted to heat treatments. Moreover, the over-aged samples were more resistant to HE than the peak-aged ones. Reverted austenite contained on the microstructure increased the fracture toughness of the material. EBSD revealed that the paths for intergranular crack propagation were mainly along grain boundaries with {001}//ND fiber orientation, while {111} and {110}//ND fibers were resistant to propagation.

1. Introduction

Maraging steels combine unique characteristics such as high strength, good toughness and formability. These steels are widely utilized in engineering applications ranging from pressure vessels operating in critical processes, aircraft components to military industry [1]. The main alloying elements of these steels are Ni, Co, Mo and Ti. Maraging steels exhibit a fully martensitic structure (BCC – body centered cubic) in the solution annealed condition due to the high nickel content and the virtual absence of carbon [1,2]. In the annealed condition, these alloys are soft and deformable with hardness in the order of 30HRC [1]. The excellent mechanical properties are obtained by aging treatment in the temperature range of 440–640 °C, which produces a precipitation hardening of intermetallic phases such as Ni_3(Ti, Mo), Ni_3Ti, μ-phase and Fe_2Mo in the martensitic matrix [1–6]. Titanium and molybdenum are the main hardening elements in these alloys. Ti is the most active element in the early stages of the aging process [4]. Aging above 500 °C can promote reversion of austenite by a diffusion-controlled decomposition reaction of martensite. The reversion of austenite and precipitation of Fe_2Mo occurs nearly at the same time as a consequence of the partial dissolution of Ni_3(Ti,Mo) [7]. This diffusion of alloying elements causes changes in the lattice parameter of the martensitic matrix [8,9]. The morphology, phase fraction and formation mechanism of reverted austenite in 18% Ni maraging steel are closely related to the aging temperature and time [7,10]. Furthermore, reverted austenite significantly influences mechanical [5,11] and magnetic properties [12,13] in these steels.

It is known that service environments may degrade the mechanical properties of ultra high strength steels [14,15]. This phenomenon is called environmentally assisted cracking (EAC). Hydrogen embrittlement (HE) is a typical example of this phenomenon in steels [16]. Hydrogen dissolved in the lattice matrix of materials can exists in dissociated form and concentrate at grain boundaries, vacancies and interstitial sites [16]. The mechanism of HE supposes that hydrogen dissolved at high concentrations decreases the cohesive force between the atoms of the alloy lattice, at grain boundaries and at interfaces, generating localized plastic deformation or cleavage, leading to the coalescence of microcracks and finally to fracture. Pressure-expand theory and decohesion model are two examples of theories that consider this type of EAC [16].

Maraging steels may suffer HE when exposed to certain environments [14,17–23]. Reddy et al. [18] and Tsay et al. [19] have independently shown that a reduction in ultimate tensile strength, elongation and area reduction occur when the hydrogen concen-

* Corresponding author. Fax: +55 85 3366 9070.
E-mail address: mgsilva@ufc.br (M.J. Gomes da Silva).

http://dx.doi.org/10.1016/j.corsci.2015.06.022
0010-938X/

Table 1
Chemical composition of 18% Ni 300 grade maraging steel.

Element	Ni	Co	Mo	Ti	Al	Fe
wt%	18.68	9.62	4.84	0.87	0.38	Bal.

tration increases in the material. Hydrogen-induced crack (HIC) propagates along both reverted austenite and martensite lath boundaries as result of enrichment in the hydrogen concentration [23]. Maraging steels in over-aged conditions exhibits higher resistance to HE in comparison to other aging conditions [19,20,23]. In this work, HE susceptibility of ultra high strength 300 grade maraging steel in solution annealed and aged conditions was studied using slow strain rate test (SSRT). Experimental evidence have shown that the HE susceptibility of the steel follows a decreasing order of peak-aged, over-aged and solution annealed conditions. The HE susceptibility depends on both strength and reverted austenite content of the materials. The fracture surface analysis revealed secondary cracks regardless of heat treatments. Electron backscatter diffraction (EBSD) was employed to show crystal orientation in the region of crack tip. It was observed the cracks propagate intergranulary along low-angle boundaries (LABs) with an orientation {001}//ND fiber shared by neighboring grains having orientations within this fiber.

2. Material and methods

2.1. Material

Ultra high strength 18% Ni 300 grade maraging steel was used in this study. The chemical composition is given in Table 1. Samples with dimension of $12 \times 11 \times 3\ mm^3$ were solution annealed at 820 °C for 1 h, air cooled to room temperature. Subsequently, samples were aged at 480 and 570 °C for 3, 10, 25 and 50 h followed by air cooling.

2.2. Microstructural characterization

X–ray diffraction (XRD) measurements were carried out on ground faces of the samples (SiC paper 200–400 mesh) using a Philips® XíPert Pro diffractometer, in step scan mode with step size 0.013°, time per step 100 s and angular interval 35–120°. CuKα (0.1540 nm) radiation was used at 40 kV and 40 mA with monochromator. Spinner was used to minimize the texture effect [12].

Eddy current measurements were performed on samples aged at 570 °C for 3, 10, 25 and 50 h. A fully martensitic solution annealed sample was used as a reference because aged samples contain some reverted austenite and precipitates which may affect the eddy current response [24,25]. An Olympus® Omniscan MX equipment operating at 700 kHz was employed for the eddy current measurements.

Microstructural examination was performed on metallographic samples ground using SiC papers with mesh size up to 1200, then polished with 6, 3 and 1 μm diamond paste and finally etched with Marbleís reagent [26]. For this investigation an Olympus® BX–51 M optical microscope and Philips® XL–30 scanning electron microscope (SEM) were used. Rockwell hardness measurements were performed using 150 kg work load.

Samples for EBSD analysis were prepared on the fractured surfaces. This involved grinding using SiC papers up to 600 mesh, subsequently polishing with 6, 3 and 1 μm diamond paste and finally 0.5 μm colloidal silica suspension was used for final polishing.

2.3. Quantitative analysis of reverted austenite

X–ray diffraction (XRD) quantitative analysis was performed by the direct comparison method [27], assuming a different chemical composition of austenite and martensite phases which can be quite different depending on the aging conditions. Different atomic scattering factors of both phases were considered [9]. Three martensite, $\{110\}\alpha$, $\{200\}\alpha$, $\{211\}\alpha$, and five austenite peaks $\{111\}_\gamma$, $\{200\}_\gamma$, $\{220\}_\gamma$, $\{311\}_\gamma$ and $\{222\}_\gamma$ were analyzed. To minimize the effect of texture, the average value of all compared diffraction peaks were calculated [12].

2.4. Slow strain rate test

To assess HE of the steel, slow strain rate tests (SSRT) were conducted with a strain rate of $1.0 \times 10^{-6}\ s^{-1}$. The tests were performed with samples in air and immersed in an aqueous 0.6 M NaCl electrolyte using a simultaneous application of potential of −1.2 V_{SCE} according to ASTM G129-00 and ASTM F1624-09 [28,29]. The relative strength and plasticity losses were chosen to identify HE susceptibility. These were calculated as described by Wang et al. [23]. Cylindrical samples of 4.1 mm in diameter and 28 mm in gauge length were employed [30]. The samples were solution annealed at 820 °C for 1 h (HRC 26.7) then aged at 480 (HRC 52.0) and 570 °C for 3 h (HRC 49.5) and finally air cooled. These conditions are named as annealed, peak-aged and over-aged, respectively and this labeled accordingly in the rest of the manuscript. All heat treatments were performed in a vacuum sealed quartz tube. The region of the samples exposed to the electrolyte were prepared using SiC paper up to 600 mesh, washed in distilled water and blow dried. Hydrogen charging was carried out in a 0.6 M NaCl electrolyte under potentiostatic control at −1.2 V_{SCE} at room temperature. The average cathodic current density of $0.32\ mAcm^{-2}$ was observed. The reference electrode was a satured calomel electrode (SCE), and the counter-electrode was a platinum bar (diameter 4.0 mm, length 50 mm). A potentiotast Verstat 3 with current booster of 2 A was used to apply the potential. The samples were charged for 24 h before and during the SSRT. The tests were performed in a Cortest® machine model CERT (Constantís Extension Rate Test) with a load cell of 44 kN. The fractured surfaces of samples after SSRT were examined using a Shimadzu scanning electron microscope (SEM). In addition, crystal orientation maps were obtained using an EBSD on a Philips® XL–30 SEM equipped with HKL Oxford® camera using Channel 5 software.

3. Results and discussion

3.1. Microstructural characterization

XRD results from samples after the following heat-treatment: solution annealed at 820 °C for 1 h and aged at 570 °C for different periods of time are shown in Fig. 1(a). Only a BCC structure was found in the solution annealed samples. In the samples aged at 570 °C, in addition to BCC peaks, austenite FCC (face centered cubic) peaks were identified after 3 h of aging. The intensity of the austenite peaks increases with aging time. Viswanathan et al. [4] detected reverted austenite in 18% Ni maraging steel after similar aging treatments. Studies conducted by [1,3–6] showed that aging above 500 °C promotes the formation of reverted austenite in addition to the precipitation of $Ni_3(Ti,Mo)$, Ni_3Ti and Fe_2Mo intermetallic compounds. In the present study, no diffraction peaks from these phases were detected. This is presumably due to their low volume fraction that is below the detection limit of the technique (approximately 5 vol.-%) [27]. Sha et al. [4] reported that the volume fraction of Ni_3Ti and μ-phase in 300 grade maraging steel aged at

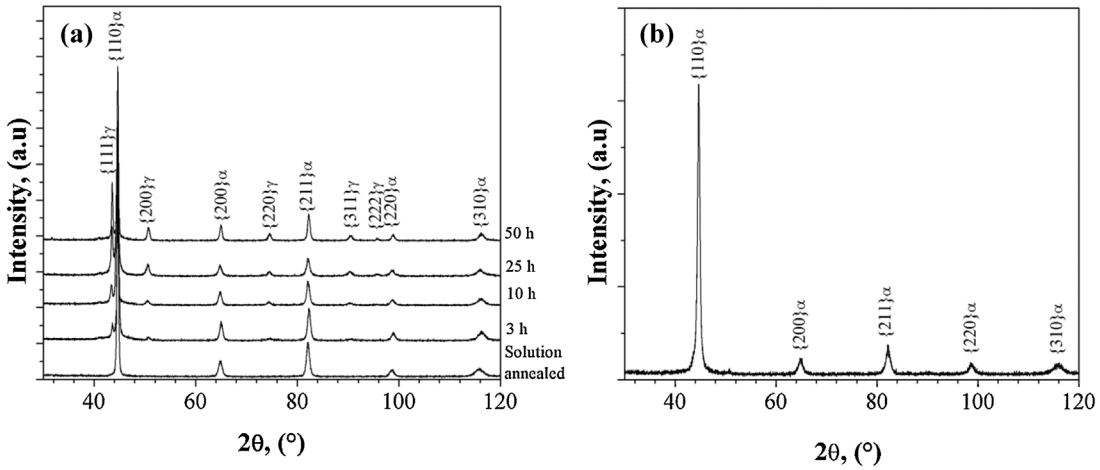

Fig. 1. (a) X-ray diffraction patterns of the samples solution annealed at 820 °C for 1 h and aged at 570 °C for 3, 10, 25 and 50 h and (b) aged at 480 °C for 50 h.

510 °C for 128 h are below 3 vol.-%. In the samples aged at 480 °C for 50 h only BCC peaks could be identified as seen in Fig. 1(b). It is assumed that at these aging conditions no reverted austenite forms or the volume fraction of the phase is too low to be detected. Rajkumar et al. [25] could not detect the formation of austenite in 18% Ni maraging steel up to 40 h of aging at 482 °C by XRD. Nonetheless they could identify about 5% of reverted austenite after aging at same temperature for 70 h.

From the XRD patterns, the volume fraction of reverted austenite was determined by the direct comparison method [27] and was plotted against aging time at the temperature of 570 °C in Fig. 2. One can observe that a reverse transformation from martensite to austenite occurs with progressing aging time. Aging up to 25 h leads to a nearly linear increase of reverted austenite, reaching 33.3 vol.-%. Further aging (50 h) leads to a slight increase to 36.1 vol.-%.

In order to understand the formation process of reverted austenite in maraging steels it is important to consider the distribution of alloying elements in the martensitic matrix during aging treatments. The thermodynamic simulation performed indicated that reverted austenite is rich in Ni and Mo [4]. It is suggested that reverse transformation from martensite to austenite is controlled by both Ni and Mo elements in martensite phase. Li and Yin [7] observed reverted austenite at grain and along martensite laths boundaries as well as plate like austenite within the martensite laths. They also concluded that the Ni from dissolved $Ni_3(Ti,Mo)$ precipitates is used to form reverted austenite while Mo is used to form Fe_2Mo phase. EDS analyses confirmed that reverted austenite was enriched in Ni [7,10].

Eddy current measurements were performed in samples aged at 570 °C for 3, 10, 25 and 50 h as shown Fig. 3. During the first 10 h of aging, impedance modulus drops quickly which can be associated with the reversion of austenite. Then, with progressing aging the impedance modulus changes at a lower rate. This can be attributed to the large volume fraction of reverted austenite formed under this condition. Similar results were found by Habiby et al. [24]. Rajkumar et al. [25] observed that for longer aging periods eddy current induced voltage changed gradually as a result of an increase in the volume fraction of reverted austenite.

Microstructural examinations revealed a typical martensitic microstructure in samples solution annealed at 820 °C for 1 h and aged at 480 °C for all periods of time. No reverted austenite was observed under these conditions. However, after aging at 570 °C for 3 h austenitic phase was identified. Fig. 3 shows white needles of reverted austenite along martensitic lath boundaries, which is consistent with Farooq et al. [26] findings.

3.2. SSRT and HE susceptibility

Typical SSRT stress-strain curves of samples (i) solution annealed at 820 °C for 1 h (annealed), (ii) solution annealed and aged at 480 °C for 3 h (peak-aged) and (iii) solution annealed

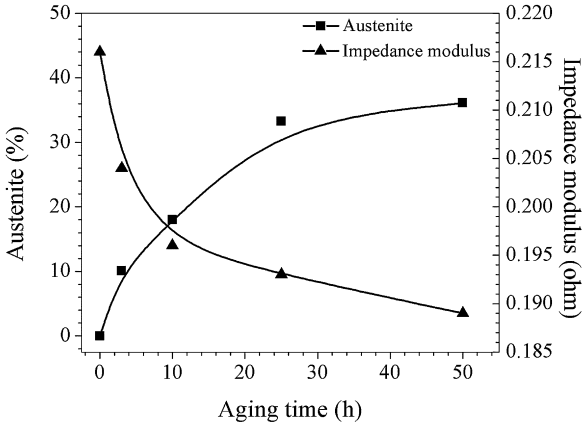

Fig. 2. Volume fraction of reverted austenite and impedance modulus against aging time.

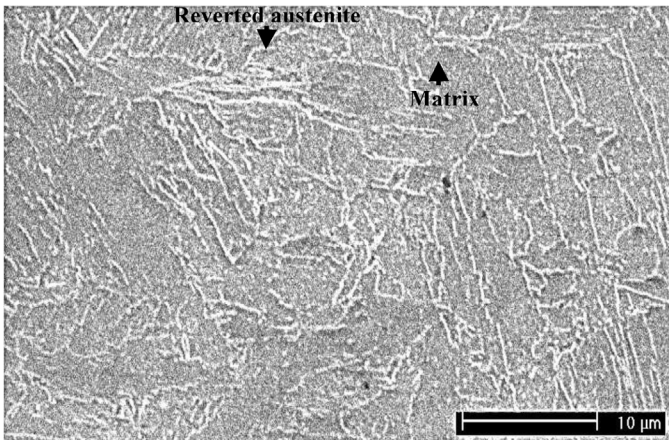

Fig. 3. SEM SE micrographs of sample aged at 570 °C for 3 h.

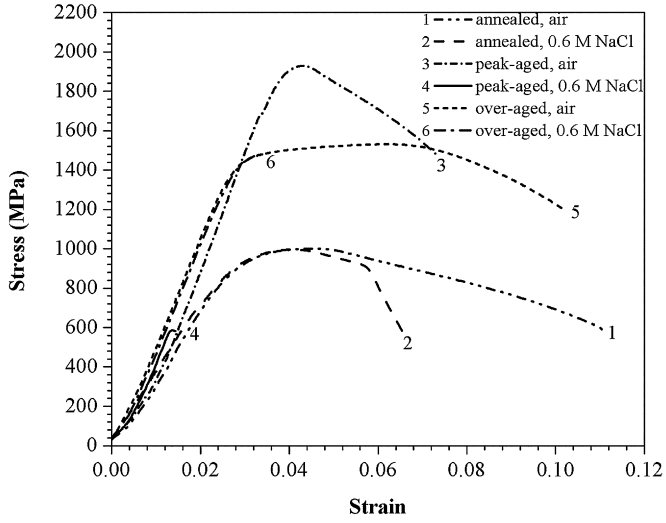

Fig. 4. SSRT stress–strain curves for solution annealed and aged samples at different conditions in air and during dynamic hydrogen charging in 0.6 M NaCl solution under cathodic potential.

and aged at 570 °C for 3 h (over-aged) tested in air and during dynamic hydrogen charging are presented in Fig. 4. The mechanical properties of the samples changed with aging treatment and hydrogen charging. In air, the samples in all heat treatment conditions showed ductile behavior with a necking preceding the fracture. The peak-aged samples had the highest ultimate tensile strength (UTS) whereas the samples in annealed condition presented higher ductility, as observed in Fig. 4. This figure also revealed that reversion of austenite in the over-aged samples decreases UTS and increases the ductility.

However, a significant reduction of mechanical properties during SSRT hydrogen charging was observed for all samples tested. Fracture occurs when K_I reaches a critical value, K_{Ic}, which is a material property and predicts that the fracture stress σ_f is given by [31]:

$$\sigma_f = \frac{K_{Ic}}{\sqrt{\pi\alpha}} \quad (1)$$

where, α, is the size of the crack present in the microstructure [31]. The value of σ_f for the peak aged sample in the presence of hydrogen is less than 1/3 of the ultimate strength measured when tested in air. The value of σ_f in the sample over-aged, with reverted austenite present in the microstructure, is the same as of the ultimate strength measured when tested without hydrogen. The presence of reverted austenite in the microstructure elevated significantly the fracture toughness K_{Ic} increasing the value for crack propagation [32].

Table 2 shows mechanical properties of the material tested in air and in 0.6 M NaCl solution at −1.2 V_{SCE} in addition to calculated parameters affected by HE. As can be seen in Table 2, values of the relative elongation (HE (δ)), the relative reduction in area of cross section (HE (ψ)) and the relative strength (HE (UTS)) are lower in the annealed samples. This is additionally supported by the longest time to fracture in this condition. Therefore this treatment results in better resistance to HE. In contrast, the peak-aged samples are more susceptible to HE. The over-aged samples showed in comparison to peak aged specimens lower HE susceptibility due to the presence of reverted austenite ~10 vol.-%, as showed in Fig. 2. Another important observation is that the HE susceptibility increases with the strength of the material and decreases with the reverted austenite content, in good agreement with studies of Rao et al.[14], Reddy et al. [18], Tsay et al. [20], and Wang et al. [23].

3.3. Fracture surface examination

After the SSRT experiments, fracture surfaces of samples were studied using SEM, Fig. 5(a–f). Low magnification fractographs of annealed, peak-aged and over-aged samples after SSRT in air are shown in Fig. 5(a–c). Regardless the heat treatment, the samples exhibited extensive plastic deformation (necking) around the fracture surrounded by the shear lip with typical ductile failure behavior. In contrast, a brittle fracture behavior was observed in same samples tested during the hydrogen charging in 0.6 M NaCl solution with minimal necking at the fracture as presented in Fig. 5(d–f).

High magnification view of solution annealed sample tested in air, Fig. 6(a), revealed coarse dimples responsible for ductile fracture. The same type of fracture was observed in peak-aged and over-aged samples tested in air. High magnification SEM fractographs of annealed and over-aged samples tested during hydrogen charging in 0.6 M NaCl environment revealed that the fractographic features of the samples changed from ductile dimples to a mixture of ductile dimples and quasi-cleavage planes suggesting a mixed mode of fracture, as shown in Fig. 6(b). In addition, after dynamic hydrogen charging, secondary cracks were observed regardless of heat treatments, as displayed in Fig. 6(b–d). Hydrogen dissolved at high concentration decreases the cohesive force between atoms quasi-cleavage regions [16]. Intergranular fracture was observed in peak-aged samples, as presented in Fig. 6(c). At a low strain rate, diffusion and concentration of hydrogen into the material is predominantly at grain boundaries [20,23]. This promotes intercrystalline fracture [20], and propagation along the martensite lath boundaries [23] in maraging steels. Previous studies have showed that at high strength conditions maraging steels have been most susceptible to HIC [14,18]. Reddy et al. [18] reported that the transition from ductile to brittle mode in 250 grade maraging steel is caused by the increase of hydrogen absorbed. In over-aged samples, Fig. 6(d), a quasi-cleavage fracture was observed.

Fig. 7(a) shows secondary cracks induced by hydrogen in the polished fracture surface of the peak-aged sample. Fig. 7(b) shows the crystal orientation in the region of crack tip and the inverse pole figure (IPF) in Fig. 7(c). It can be concluded that the crack propagates along grain boundaries related to {001}//ND fiber orientation (red-grains colored). Moreover, Venegas et al. [33] proved that high angle grain boundaries with higher stored energy related to {001}//ND

Table 2
Mechanical properties of 18% Ni 300 grade maraging steel tested on air and in 0.6 M NaCl at −1.2 V_{SCE} at room temperature. In this table the symbols mean; δ: elongation; ψ: reduction in area of cross section; HE $(X) = [(X_{air} - X_{0.6\,MNaCl})/X_{air}] \times 100$ where X is property under investigation.

Medium	Condition	UTS (MPa)	δ (%)	ψ (%)	HE (UTS) (%)	HE (δ) (%)	HE (ψ) (%)	Time to fracture (h)
Air	Annealed	1005	11.0	61.3	–	–	–	34.5
	Peak-aged	1950	8.0	36.3	–	–	–	29.2
	Over-aged	1496	9.7	39.8	–	–	–	34.2
0.6 M NaCl	Annealed	1000	6.6	9.9	0.5	40.0	83.6	21.6
	Peak-aged	613	1.7	2.7	68.6	78.7	92.6	7.4
	Over-aged	976	2.6	5.5	34.8	73.2	86.2	4.5

The values presented in the table are average of three measurements.

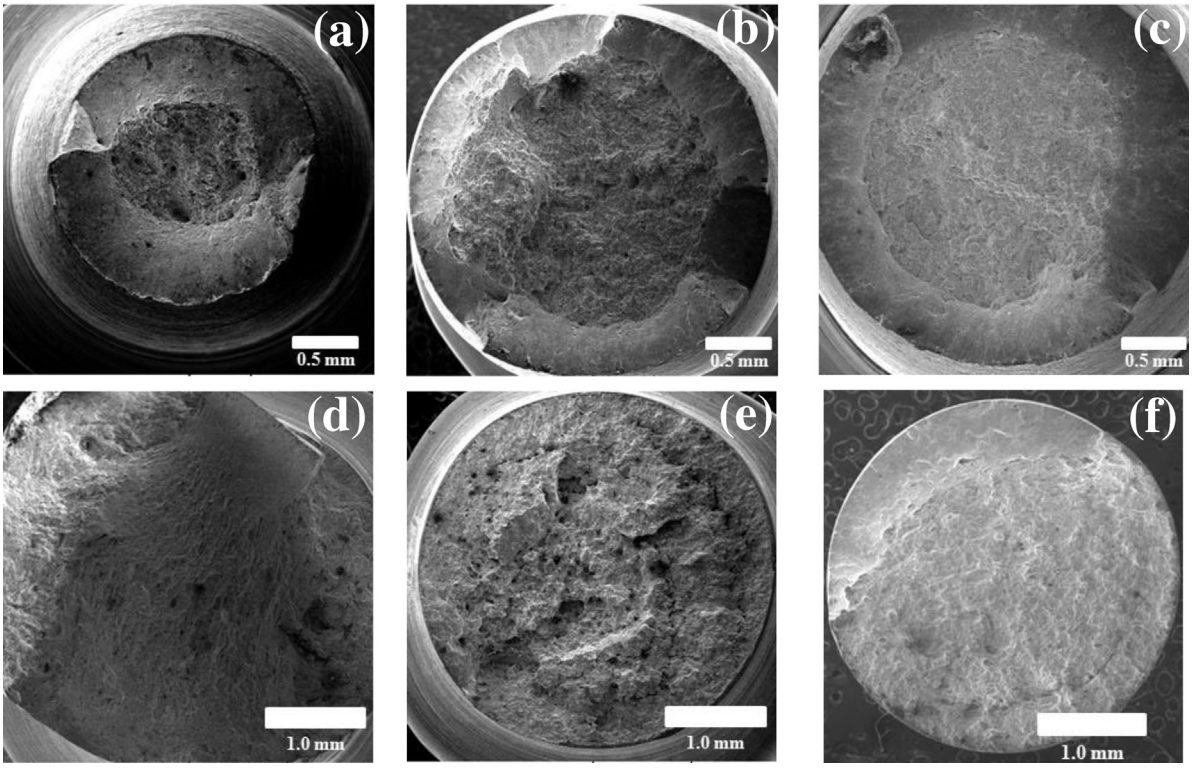

Fig. 5. Low magnification SEM SE fractographs of samples (a) annealed, (b) peak-aged and (c) over-aged tested in air and (d) annealed, (e) peak-aged and (f) over-aged tested in 0.6 M NaCl solution under cathodic potential.

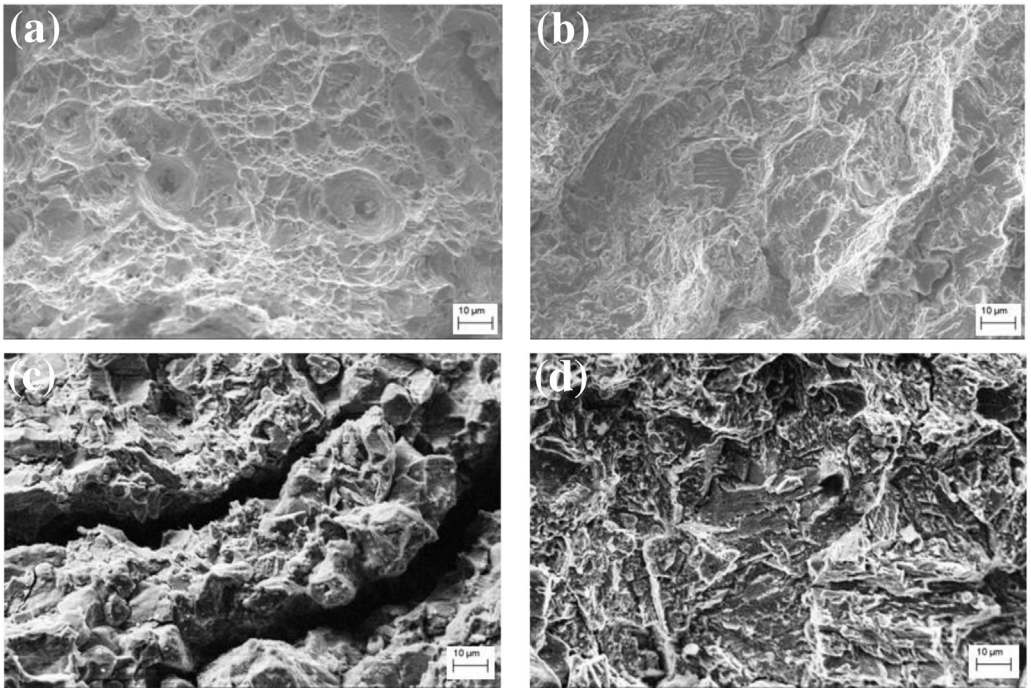

Fig. 6. High magnification SEM SE fractographs of sample (a) solution annealed tested in air and (b) solution annealed, (c) peak-aged and (d) over-aged tested in 0.6 M NaCl under cathodic potential.

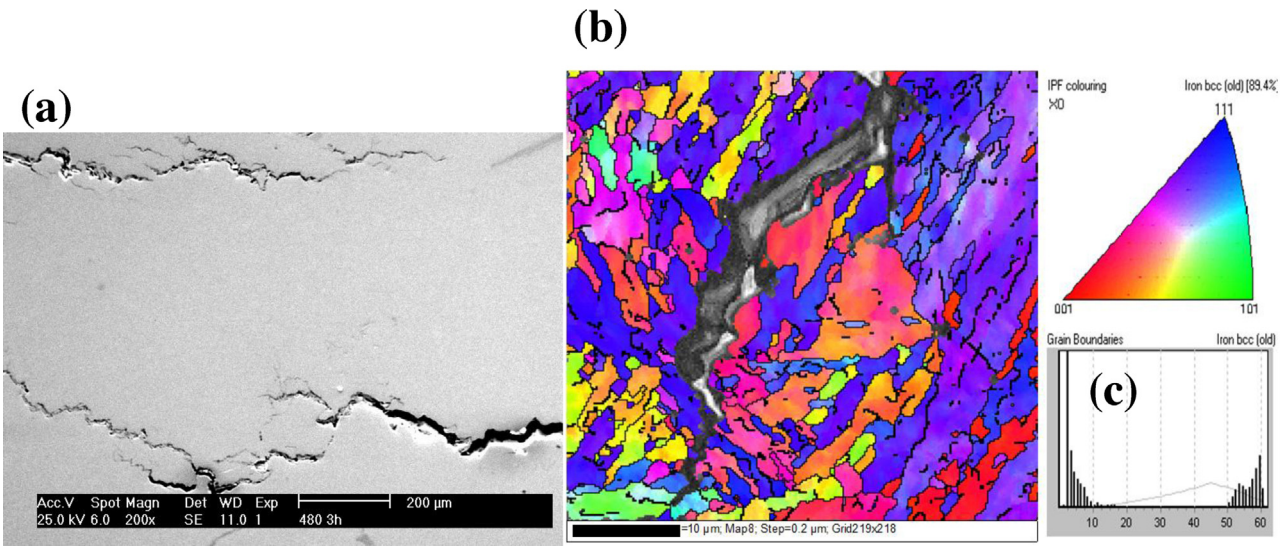

Fig. 7. (a) SEM SE microphaph of polished fracture surface of peak-aged sample showing secondary cracks induced by hydrogen and (b) EBSD orientation map from the sample shown in (a) with corresponding standard IPF color triangle, (c) grain misorientation distribution.
Tables

is preferenced to crack nucleation. On the other hand, {111} and {110}//ND fibers are known to show a high resistance to crack propagation [34], so cracks can be stopped at these boundaries. These results are in good agreement with [23,34].

4. Conclusions

Hydrogen embrittlement (HE) in ultra high strength 300 grade maraging steel in solution annealed, peak-aged and over-aged condition was studied by SSRT in air and in aqueous 0.6 M NaCl at −1.2 V_{SCE} environments. Based on the experiments the following conclusions can be drawn:

1. The steel is prone to HE in all heat treatment condition under investigation. The ranking of HE susceptibility in the decreasing order was peak-aged, over-aged and solution annealed condition. The HE susceptibility depends on both the material strength and reverted austenite content.
2. Fracture surface showed a mixture of ductile mode and quasi-cleavage fracture on solution annealed and over-aged samples. However, large regions of intergranular fracture were observed in peak-aged samples. Therefore hydrogen implied greatest damage on steel in peak-aged condition.
3. The reverted austenite present in the over-aged samples increased the fracture toughness (K_{Ic}) of the material increasing its failure stress.
4. The paths for intergranular crack propagation in this material were mainly in grain boundaries along {001}//ND fiber orientation, while {111} and {110}//ND fibers were more resistant to crack propagation.

Acknowledgments

This work was supported by Coordenação de Aperfeiçoamento de Pessoal de Nível Superior - CAPES. The authors would like to acknowledge experimental support provided by the Instituto Nacional de Tecnologia (INT), Brazil and the Universidade Federal do Espírito Santo (Marcelo Macêdo and Schérlio Scandian), Brazil.

References

[1] A. Magnée, J.M. Drapier, J. Dumont, D. Coutsouradis, L. Habraken, Cobalt-containing high-strength steels, in: Centre d'Information du Cobalt, Brussels, 1974.
[2] S. Floreen, R.F. Decker, Heat treatment of 18% Ni maraging steel, Trans. ASM 55 (1962) 518–530.
[3] V.K. Vasudevan, S.J. Kim, C.M. Wayman, Precipitation reactions and strengthening behavior in 18wt pct nickel maraging steels, Metall. Trans. A 21 (1990) 2655–2668.
[4] W. Sha, A. Cerezo, G.D.W. Smith, Phase chemistry and precipitation reactions in maraging steels: Part I. Introduction and study of Co-containing C-300 steel, Metall. Trans. A 24 (1993) 1221–1232.
[5] U.K. Viswanathan, G.K. Dey, M.K. Asundi, Precipitation hardening in 350 grade maraging steel, Metall. Trans. A 24 (1993) 2429–2442.
[6] R. Tewari, S. Mazumder, I.S. Batra, G.K. Dey, S. Banerjee, Precipitation in 18 wt% maraging steel of grade 350, Acta Mater. 48 (2000) 1187–1200.
[7] X. Li, Z. Yin, Reverted austenite during aging in 18Ni(350) maraging steel, Mater. Lett. 24 (1995) 239–242.
[8] F. Habiby, T.N. Siddiqui, H. Hussain, A.U. Haq, A.Q. Khan, Lattice changes in the martensitic phase due aging in 18% wt nickel maraging steel grade 350, J. Mater. Sci. 31 (1996) 305–309.
[9] J.M. Pardal, S.S.M. Tavares, M.P. Cindra Fonseca, H.F.G. Abreu, J.J.M. Silva, Study of the austenite quantification by X-ray diffraction in the 18Ni-Co-Mo-Ti maraging 300 steel, J. Mater. Sci 41 (2006) 2301–2307.
[10] M. Farooque, H. Ayub, A.U. Haq, A.Q. Khan, The formation of reverted austenite in 18% Ni 350 grade maraging steel, J. Mater. Sci. 33 (1998) 2927–2930.
[11] U.K. Viswanathan, G.K. Dey, V. Sethumadhavan, Effects of austenite reversion during overageing on the mechanical properties of 18 Ni (350) maraging steel, Mater. Sci. Eng. A 398 (2005) 367–372.
[12] M. Ahmed, A. Ali, S.K. Hasnain, F.H. Hashmi, A.Q. Khan, Magnetic properties of maraging steel in relation to deformation and structural phase transformations, Acta Metall. Mater. 42 (1994) 631–638.
[13] S.S.M. Tavares, H.F.G. Abreu, J.M. Neto, M.R. Da Silva, I. Popa, A thermomagnetic study of the martensite-austenite phase transition in the maraging steel, J. Alloys Compd. 258 (2003) 152–156.
[14] M.N. Rao, M.K. Mohan, P.U.M. Reddy, Environmentally assisted cracking of 18%Ni maraging, Corros. Sci. 51 (2009) 1645–1650.
[15] A.M. Elhoud, N.C. Renton, W.F. Deans, Hydrogen embrittlement of super duplex stainless steel in acid solution, Int. J. Hydrogen Energy 35 (2010) 6455–6464.
[16] R.A. Oriani, Hydrogen embrittlement of steels, Ann. Rev. Mater. Sci. 8 (1978) 327–357.
[17] P.S. Pao, R.P. Wei, Hydrogen assisted crack growth in 18Ni (300) maraging steel, Scr. Metall. 11 (1977) 515–520.
[18] K.G. Reddy, S. Arumugam, T.S. Lakshmanan, Hydrogen embrittlement of maraging steel, J. Mater. Sci. 27 (1992) 5159–5162.
[19] L.W. Tsay, W.C. Lee, W.C. Luu, J.K. Wu, Effect of hydrogen environment on the notched tensile properties of T-250 maraging steel annealed by laser treatment, Corros. Sci. 44 (2002) 1311–1327.
[20] L.W. Tsay, Y.F. Hu, C. Chen, Embrittlement of T-200 maraging steel in a hydrogen sulfide solution, Corros. Sci. 47 (2005) 965–976.

[21] L.W. Tsay, M.Y. Chi, Y.F. Wu, J.K. Wu, D.Y. Lin, Hydrogen embrittlement susceptibility and permeability of two ultra-high strength steels, Corros. Sci. 48 (2006) 1926–1938.
[22] Y.P. Zhang, D.M. Shi, W.Y. Chu, L.J. Qiao, Y.J. Shi, S.L. Zheng, S.B. Wang, Hydrogen-assisted cracking of T-250 maraging steel, Mater. Sci. Eng. A 471 (2007) 34–37.
[23] G. Wang, Y. Yan, J. Li, J. Huang, L. Qiao, A. Volinsky, Microstructure effect on hydrogen-induced cracking in TM210 maraging steel, Mater. Sci. Eng. A 586 (2013) 142–148.
[24] F. Habiby, T.N. Siddiqui, S.H. Khan, A.U. Haq, A.Q. Khan, Austenite determination by eddy current measurements in a maraging steels, NDT E Int. 25 (1992) 145–146.
[25] K.V. Rajkumar, B.P.C. Rao, B. Sasi, A. Kumar, T. Jayakumar, B. Raj, K.K. Characterization of aging behaviour in M250 grade maraging steel using eddy current non-destructive methodology, Mater. Sci. Eng. A 464 (2007) 233–240.
[26] M. Farooq, A.U. Haq, F.H. Hashmi, A.Q. Khan, Microscopic determination of austenite in 18% Ni maraging steel, Metallography 20 (1987) 377–383.
[27] D.C. Cullity, Second ed, in: Elements of X-ray Diffraction, Addison-Wesley Publishing Company, Massachusetts, 1978.
[28] ASTM standard G129-00, ASTM International, Philadelphia, PA, USA, 2000.
[29] ASTM standard F1624-09, ASTM International, Philadelphia, PA, USA, 2009.
[30] ASTM standard E8/E8M-11, ASTM International, Philadelphia, PA, USA, 2011.
[31] W.F. Hosford, First ed, in: Mechanical Behavior of Materials, Cambridge University Press, New York, 2005.
[32] R. Wu, W. Li, S. Zhou, Y. Zhong, L. Wang, X. Jin, Effect of retained austenite on the fracture toughness of quenching and partitioning (Q&P)-treated sheet steels, Metall. Mater. Trans. A 45 (2014) 1892–1902.
[33] V. Venegas, F. Caleyo, J.L. González, T. Baudin, J.M. Hallen, R. Penelle, EBSD study of hydrogen-induced cracking in API-5-L-X56 pipeline steel, Scr. Mater. 52 (2005) 147–152.
[34] V. Venegas, F. Caleyo, J.M. Hallen, T. Baudin, R. Penelle, Role of crystallographic texture in hydrogen-induced cracking of low carbon steels for sour service piping, Metall. Mater. Trans. A 38 (2007) 1022–1031.